ACS APPLIED MATERIALS & INTERFACES

Research Article

www.acsami.org

# Wetting Behavior of Ionic Liquid on Mesoporous Titanium Dioxide Surface by Atomic Force Microscopy

Rong An, Yudan Zhu, Nanhua Wu, Wenlong Xie, Jiawei Lu, Xin Feng, and Xiaohua Lu*

State Key Laboratory of Materials-Oriented Chemical Engineering, Nanjing University of Technology, 5 Xinmofan Road, Nanjing 210009, P. R. China

**ABSTRACT:** Ionic liquids based on 1-butyl-3-methylimidazolium hexafluoro-phosphate (ILs [Bmim][$PF_6$]) has been employed to wet the mesoporous and dense titanium dioxide ($TiO_2$) films. It has been found from atomic force microscopy (AFM) analysis that ILs [Bmim][$PF_6$] can form a wetting phase on mesoporous $TiO_2$ films, but nonwetting and sphere shaped droplets on dense films. AFM topography, phase images, and adhesion measurements suggest a remarkable dependence of wetting ILs [Bmim][$PF_6$] films on the $TiO_2$ porous geometry. On mesoporous $TiO_2$ films, the adhesive force of ILs [Bmim][$PF_6$] reaches at 40 nN, but only 4 nN on dense $TiO_2$ films. The weak interacting ILs [Bmim][$PF_6$] on dense $TiO_2$ films forms rounded liquid spheres (contact angle as 40°), which helps to reduce friction locally but not on the whole surface. The stronger adhesive force on mesoporous $TiO_2$ films makes ILs [Bmim][$PF_6$] adhere to the surface tightly (contact angle as 5°), and this feature remains after five months. The stable spreading ILs [Bmim][$PF_6$] films provide low friction coefficient (0.0025), large wetting areas, and short $CO_2$ diffusion distance on the whole mesoporous $TiO_2$ surface, avoiding the significant decelerating effect through equilibrium limitations to enable $CO_2$ capture rate up to 1.6 and 10 times faster than that on dense $TiO_2$ and pure ILs, respectively. And importantly, ILs wetted on mesoporous $TiO_2$ shorten the time reaching to the maximum adsorption rate (2.8 min), faster than that on mesoporous $TiO_2$ (6.1 min), and dense $TiO_2$ (11.2 min). This work provides an important guidance for the improvement of the efficiency of $CO_2$ capture, gas separation, and the lubrication of micro/nanoelectromechanical systems (M/NEMs).

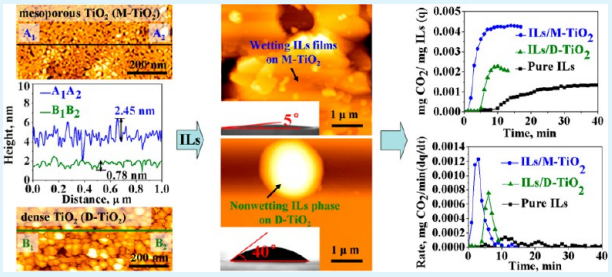


**KEYWORDS:** *ionic liquid, mesoporous $TiO_2$, wetting, AFM, adhesive force, friction, $CO_2$ capture*

## 1. INTRODUCTION

Ionic liquids (ILs) are ionic compounds consisting of large organic cations and various kinds of anions that exist in the liquid state over a wide temperature range.[1] ILs possess unique and desirable physicochemical properties, such as high chemical and thermal stabilities, low vapor pressure, high thermal conductivity, and excellent solubility for a wide range of organic and inorganic compounds.[2−4] Therefore, ILs have attracted considerable interests in various fields,[5] such as $CO_2$ capture,[6,7] gas separation,[8,9] and energy production/storage.[10] Recently, ILs have been considered as a new promising class of lubricants that could significantly improve the wear life in micro/nanoelectromechanical systems (M/NEMs).[11−13] However, there are still some challenges, such as corrosion and oxidation,[14,15] while using in different systems, including solvents for synthesis and catalysis,[4] dye-sensitized solar cells,[16] lubricating oils,[14,17] $CO_2$ separation,[7] and so on. Among all these cases, in essence, the device performance strongly depends on the wetting behavior at interface between ILs and solid surfaces.[5] The durability of IL films on various substrates has been explored from the standpoint of film formation (wettability).[18] Many strategies,[19] such as solidification with gelating agents[16,20] and nanoparticles,[21] the incorporation of ILs into polymer networks,[22] confinement in inorganic gels,[23] etc., have been investigated to solidify the ILs into self-supporting solid surfaces. Nevertheless, it has been proved that many advantages of a pure IL would be obviated when adding these materials.[24] Moreover, these treatments based on polymers and organic gels, just like organic self-assembled monolayers (SAMs), are susceptible to oxidization, hydrolyzation, or degradation.[25−27]

Titanium (Ti) has been acknowledged as a favorable structural material and used in many fields because of its high mechanical strength, low density, and excellent anticorrosion property.[28,29] Generally, a native dense titanium dioxide ($TiO_2$) layer[30−32] could form on the Ti surface, which prevents the bulk Ti from further corrosion and oxidation. That is to say, the $TiO_2$ layer on Ti could conquer the foresaid challenges in ILs applications, for example, identified corrosion and oxidation.[14,15] However, the dense $TiO_2$ films formed on Ti can not support ILs in the form of well-packed layers. To solve the problem, we adopted a promising approach that the porous solid matrix could immobilize ILs[33] as stable films. The idea was enlightened by the fact that a fishing net can support water

Received: January 15, 2013
Accepted: March 6, 2013
Published: March 6, 2013

  

films on its millimeter-sized holes.[34] We replaced the dense $TiO_2$ films by mesoporous $TiO_2$ films to provide porous surface matrix to further immobilize ILs. Combined with the high sensitivity in nanoscale,[35,36] atomic force microscopy (AFM) offers an effective way to explore the molecular-level factors governing IL behavior on various surfaces.

In this work, we report on the direct observation of wetting behavior of 1-butyl-3-methylimidazolium hexafluoro-phosphate ([Bmim][$PF_6$]) layers on mesoporous $TiO_2$ films by AFM. The performance characteristic of the ILs wetted on developed mesoporous $TiO_2$ materials for $CO_2$ adsorption was further determined by quantitative analysis of TG (thermogravimetry) apparatus. Noting that [Bmim][$PF_6$], not an excellent $CO_2$ adsorbent, being studied extensively, can serve as well-defined model systems to study the behavior of surfaces on the ILs and the effects on $CO_2$ adsorption. In comparison, the $CO_2$ adsorption performance of the ILs on dense $TiO_2$ is also explored.

## 2. EXPERIMENTAL SECTION

Both of the mesoporous $TiO_2$ (M-$TiO_2$) and dense $TiO_2$ films (D-$TiO_2$) could be prepared by the methods as reported previously.[37] Both films are employed as the substrate to adsorb a prototype ionic liquid (1-butyl-3-methylimidazolium hexafluoro-phosphate, [Bmim]-[$PF_6$]). The ILs [Bmim][$PF_6$] concentration in acetone solution was typically kept below $1 \times 10^{-3}$ mg/mL. The M-$TiO_2$ and D-$TiO_2$ films were immersed in the IL solutions and equilibrated for 6 h. Then they were taken out, allowing acetone to completely evaporate in air, leaving behind IL layers and droplets. To make the acetone evaporation process slower and obtain uniform coatings, the samples were cured in a saturated acetone atmosphere during evaporation.

An Autoprobe CP-Research AFM with an atomic head of 100 × 100 $\mu m^2$ scan range from Bruker Instruments was used. The AFM was operated in contact and tapping mode in air by silicon cantilevers with the spring constants of 0.01−0.5 N/m. Typically, image scan size was between 1 $\mu$m × 1 $\mu$m and 5 $\mu$m × 5 $\mu$m with scan speed of 1.00 Hz. AFM data have been analyzed by the second order flattening using Proscan (version 2.1) software.

The force measurements were performed in contact mode. A force−distance curve could be obtained in contact mode. The cantilever is bent up during approach, while during retraction, it is bent down. And then the cantilever will restore its original state as soon as the tip overcomes adhesive force from the surface. The adhesive force, that is, pull-off force, is the force jump during retraction.[38] Measured values were reproducible for five identical samples (over five independent positions for each sample, in air, at 25 °C, relative humidity ∼47%, and only the retract part of the force curves is shown here).

The friction force was measured as the probe scanned the surface along the *x*-axis. The lateral force increases linearly with the normal force for Si tip and the $TiO_2$ films. Measured values were reproducible for five identical samples (over five independent measurements for each sample, in air, at 25 °C, relative humidity ∼47%).

The specimen (M-$TiO_2$ and D-$TiO_2$ films) morphologies were evaluated by Field emission scanning electron microscopy (FESEM) using a Hitachi S-4800 (FEI, Japan) system at room temperature (20 ± 2 °C).

Raman spectroscopy was carried out on a Horiba Labram HR 800 Raman spectroscope (514 nm He−Cd laser, laser power: 20 mW) to detect the crystalline phases existing in M-$TiO_2$ and D-$TiO_2$ films.

Contact angles were measured by a SL200B (Solon technology science Co, China) at room temperature and ambient humidity. Six drops of water were placed on each sample using a manual syringe fixture. To further confirm the reproducibility, three samples were tested for both M-$TiO_2$ and D-$TiO_2$ films.

The weight changes for $CO_2$ adsorption on pure ILs [Bmim][$PF_6$] and on ILs [Bmim][$PF_6$] immobilized on mesoporous $TiO_2$ and dense $TiO_2$ over a constant temperature 35 °C are monitored by thermogravimetry (TG) analysis in a thermobalance (TG/c-DTA, Netzsch, Germany). Prior to that, each specimen needed nitrogen ($N_2$) purging for 30 min.

## 3. RESULTS AND DISCUSSION

The Raman spectrum of the M-$TiO_2$ films is shown in Figure 1 together with that of D-$TiO_2$ films for comparison. The

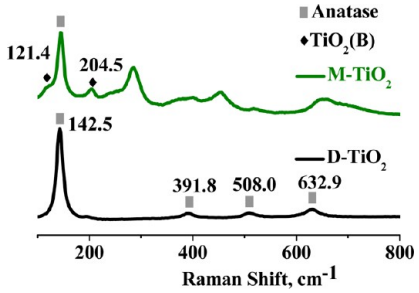


**Figure 1.** Raman spectra of the M-$TiO_2$ and D-$TiO_2$ films. The Raman vibrational bands of anatase phase are marked in solid squares and $TiO_2$-B phase are marked in solid diamonds.

structure which shows identical Raman spectra was identified as anatase at 142.5, 391.8, 508.0, and 632.9 $cm^{-1}$, in both M-$TiO_2$ and D-$TiO_2$ films. Notably in M-$TiO_2$ films, exposure of potassium dititanate ($K_2Ti_2O_5$) films to water vapor, followed by ion exchange and sintered at 500 °C, produced a crystalline solid which exhibits the distinct Raman spectra at 121.4 and 204.5 $cm^{-1}$ due to $TiO_2$-B phase. The $TiO_2$-B phase is beneficial to the mesoporous $TiO_2$ thermal stability[39] and different from the phases of anatase, rutile, and brookite $TiO_2$.[40,41]

To further investigate the two $TiO_2$ films, the surface morphologies of the M-$TiO_2$ and D-$TiO_2$ films were studied by AFM where nanopores (∼15−20 nm) and packed particles (∼50 nm) were observed on M-$TiO_2$ (Figure 2a) and D-$TiO_2$ (Figure 2b), respectively. The cross sectional line profile $A_1A_2$ in Figure 2c shows the presence of pores along the M-$TiO_2$ surface that are ∼20 nm in width and ∼2.45 nm in depth on a scanned area equivalent to 1 $\mu m^2$. The observed line profile $B_1B_2$ on D-$TiO_2$ surface (Figure 2d) is relatively flat with particles that are ∼50 nm in width and ∼0.78 nm in height on a 1 $\mu m^2$ scanned area. The contracts come from the different viscoelastic properties and surface energy of the materials[42−44] in AFM phase images. Therefore, different surface morphologies for these two types of $TiO_2$ surfaces were further demonstrated by the phase images in Figure 2e and 2f to further distinguish the features. The distributed nanopores phases are clearly observed on the M-$TiO_2$ films in Figure 2e. In contrast, the homogeneously distributed nanoparticles are seen on the D-$TiO_2$ films as shown in Figure 2f. The M-$TiO_2$ and D-$TiO_2$ films were also examined by FESEM images in Figure 2g and 2h. These observations are in agreement with those detected by AFM measurements which demonstrate that the M-$TiO_2$ films surface has a high degree of pores with diameters of about 15−20 nm and D-$TiO_2$ films consist of densely packed particles of about 50 nm.

When a a rigorous protocol for the statistical analysis of AFM images is applied, quantitative information on the structural properties of ILs [Bmim][$PF_6$] films can be obtained. Figure 3 shows the AFM topographies of [Bmim][$PF_6$] coatings on M-$TiO_2$ and D-$TiO_2$ films as well as their corresponding statistic

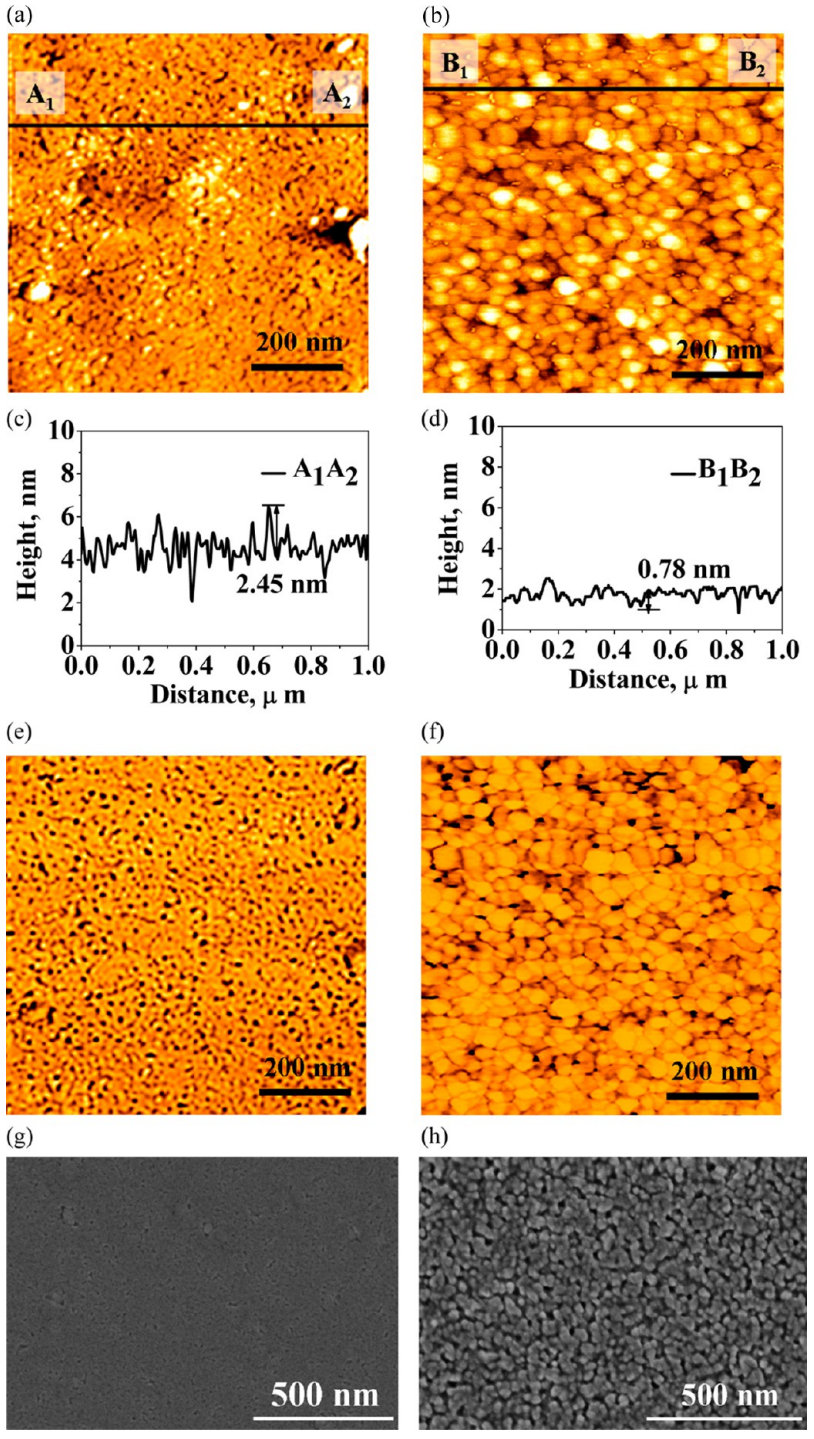


**Figure 2.** AFM topographic images of (a) M-$TiO_2$ and (b) D-$TiO_2$ films, respectively. The line profiles along the (c) $A_1A_2$ line and (d) $B_1B_2$ line, respectively. The corresponding AFM phase images of (e) M-$TiO_2$ and (f) D-$TiO_2$ films. The FESEM images of (g) M-$TiO_2$ and (h) D-$TiO_2$ films. The vertical scales are 12 nm in panels a and b and 54° in panels e and f.

results. Figure 3a shows multilayer stacking of ILs [Bmim]-[$PF_6$] wetting on M-$TiO_2$ films. It is different from the ILs behavior revealed on D-$TiO_2$ films, which exhibits nonwetting phase on rounded domains in Figure 3b. Figure 3c is the height profile along the line $T_1T_2$ in Figure 3a, which shows that the thickness of each [Bmim][$PF_6$] layer is in different multiples of 5−150 nm range on M-$TiO_2$ films. While the ILs [Bmim][$PF_6$] aggregate themselves as rounded domains on D-$TiO_2$ films and the height could even reach 413.1 nm shown in the line profile $T_3T_4$ (Figure 3d). The adhesion behavior of ILs [Bmim][$PF_6$] on the M-$TiO_2$ films is provided in Figure 3e. The adhesive force of ILs [Bmim][$PF_6$] on D-$TiO_2$ films is also shown in Figure 3f for a comparison. It is observed that the adhesive force of ILs [Bmim][$PF_6$] on M-$TiO_2$ is stronger (38.3 nN) than on D-$TiO_2$ (3.9 nN). Hence, the stronger adhesive force further lead to M-$TiO_2$ films being easily occupied by multilayer stack of [Bmim][$PF_6$] wetting phases. However, the ILs [Bmim][$PF_6$] aggregate together on D-$TiO_2$ films, showing a more pronounced tendency to form nonwetting phases. The adhesion distribution of ILs [Bmim][$PF_6$] on M-


dx.doi.org/10.1021/am400175z | ACS Appl. Mater. Interfaces 2013, 5, 2692−2698

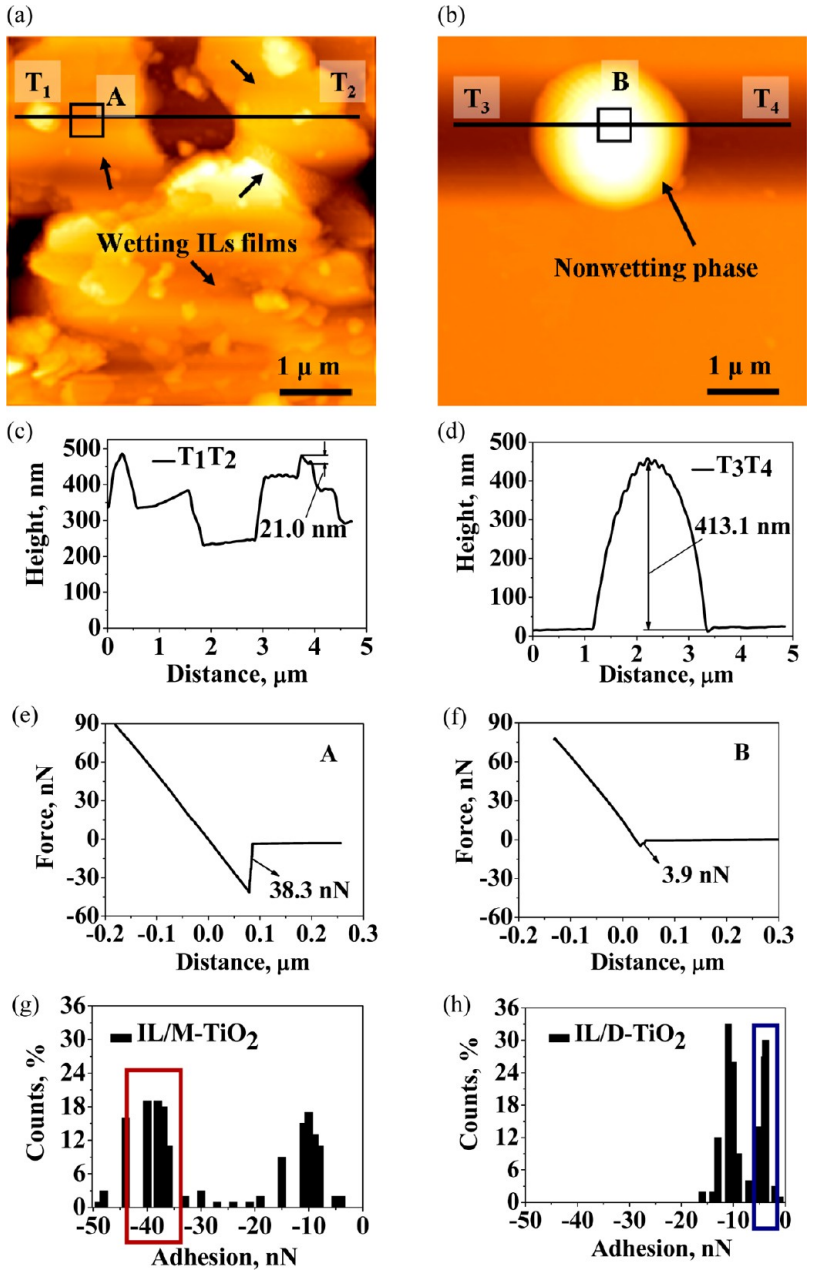


**Figure 3.** AFM topographic images of ILs [Bmim][$PF_6$] on (a) M-$TiO_2$ and (b) D-$TiO_2$ films, respectively. The line profiles along the (c) $T_1T_2$ line and (d) $T_3T_4$ line, respectively. The adhesive forces measured at (e) the points A on M-$TiO_2$ films and (f) the point B on D-$TiO_2$ films, where A and B are on the top of ILs [Bmim][$PF_6$]. The histogram of adhesive forces measured at ~155 different positions on the area of 5 $\mu$m × 5 $\mu$m of (g) M-$TiO_2$ and (h) D-$TiO_2$ films, respectively. The vertical scales in panels a and b are 600 nm.

$TiO_2$ films is shown in Figure 3g. We observe a bimodal distribution, that is, heterogeneous distribution,[45] centered around 40 and 10 nN, respectively, because of the ILs [Bmim][$PF_6$] and the $TiO_2$ films.[37] Figure 3h also shows a heterogeneously[45] bimodal adhesion distribution of ILs [Bmim][$PF_6$] on D-$TiO_2$ films, which centers around 10 and 4 nN corresponding to the $TiO_2$ films[37] and ILs [Bmim][$PF_6$], respectively. Apparently, ILs [Bmim][$PF_6$] can form a wetting films on M-$TiO_2$ films by stronger interactions, while a round nonwetting sphere on D-$TiO_2$ films formed due to weaker interfacial interactions. Noting that the observed layers on M-$TiO_2$ and D-$TiO_2$ films have been imaged again after five months, and no changes on structure and topography have been observed. This demonstrates the features of ILs [Bmim][$PF_6$] spreading out on M-$TiO_2$ films are extremely stable even in ambient (humid) conditions. [Bmim][$PF_6$] remains its weak wettability on D-$TiO_2$ films. According to the viewpoints in the literature,[34] the mesoporous surface topography of M-$TiO_2$ films may be very critical in determining the adhesion of ILs [Bmim][$PF_6$] on M-$TiO_2$ surface as a wetting phase.

Figure 4 shows simultaneously recorded topographic and phase images of a region of [Bmim][$PF_6$] coating on M-$TiO_2$ and D-$TiO_2$ films. The entrapment and immobilization of ILs [Bmim][$PF_6$] on M-$TiO_2$ films are likely to "freeze" to form a multilayered wetting phase in Figure 4a, whereas sphere-shaped nonwetting phase is formed on D-$TiO_2$ films (Figure 4b). The "freezing" of ILs [Bmim][$PF_6$] on M-$TiO_2$ films, which


dx.doi.org/10.1021/am400175z | ACS Appl. Mater. Interfaces 2013, 5, 2692−2698

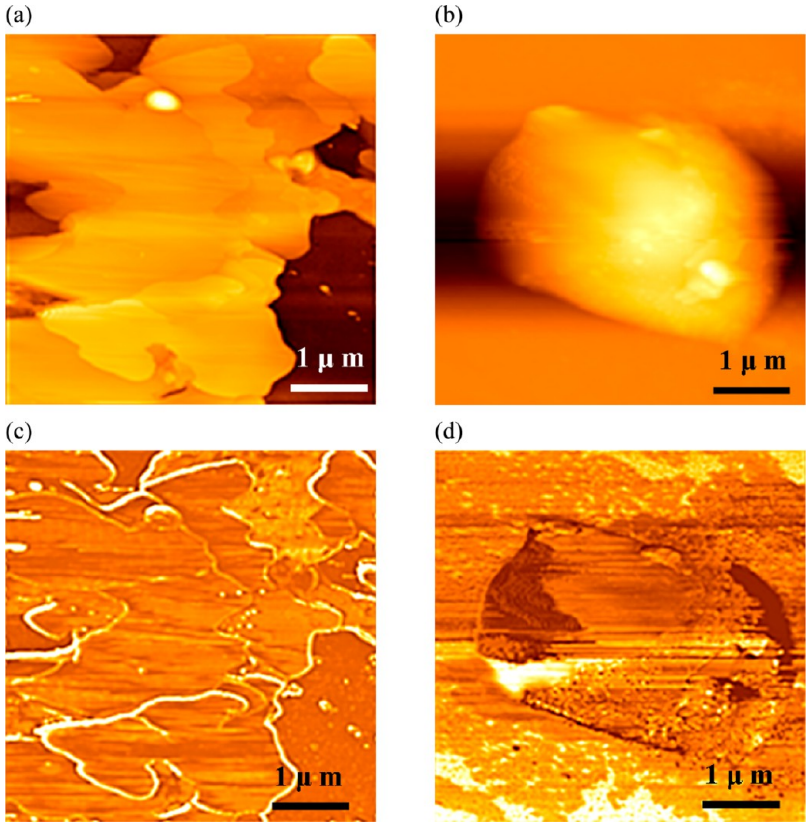


**Figure 4.** AFM topographic images of ILs [Bmim][$PF_6$] on (a) M-$TiO_2$ and (b) D-$TiO_2$ films, respectively. AFM phase images of ILs [Bmim][$PF_6$] on (c) M-$TiO_2$ and (d) D-$TiO_2$ films. The vertical scales are 80 nm in panels a and b and 36° in panels c and d.

consisted of 15−20 nm pores, exhibits a rich phase behavior that depends on the existence of the pores in nanoscale.[46,47] It can be noticed in Figure 4c and 4d that a contrast between the IL layers, droplets, and $TiO_2$ films, which suggests that the ILs and $TiO_2$ are present in different phases. In Figure 4c, the comparison of phase signal of different materials (ILs [Bmim][$PF_6$] and $TiO_2$ films) indicates the ILs [Bmim][$PF_6$] phase (area surrounded by the white lines) are able to wet M-$TiO_2$ films well. Figure 4d shows the phase contrast between ILs [Bmim][$PF_6$] and D-$TiO_2$ films. It can be found that the elliptical region, representing the aggregating ILs [Bmim][$PF_6$] phase shown on D-$TiO_2$ films in Figure 4b.

Figure 5 shows the optical micrographs of ILs [Bmim][$PF_6$] droplets on the two different $TiO_2$ surfaces. On M-$TiO_2$ surface, the ILs [Bmim][$PF_6$] droplet shows the contact angle of 5°, consistent with the IL wetting phenomenon shown in Figures 3a and 4a and 4c. However, the ILs [Bmim][$PF_6$] droplet has the contact angle of 40°, which corresponds to the nonwetting IL sphere shown in Figures 3b and 4b and 4d.

The friction coefficients of ILs [Bmim][$PF_6$] on M-$TiO_2$ and D-$TiO_2$ films as a function of lateral force for Si tip at various normal loads are shown in Figure 6. It can be found that the friction coefficients of ILs [Bmim][$PF_6$] on both of the $TiO_2$ films determined from the slopes of lateral force vs normal load plots are comparable (0.0025 for M-$TiO_2$ films, and 0.0026 for D-$TiO_2$ films). The observation indicates that tip can slip easily with the existence of ILs [Bmim][$PF_6$]. On M-$TiO_2$ films, ILs [Bmim][$PF_6$] possess a more pronounced tendency to form wetting phases, acting as excellent lubricant to further make the friction coefficient low. This is beneficial to surface adsorption and the surface in equilibrium to update to obtain a new

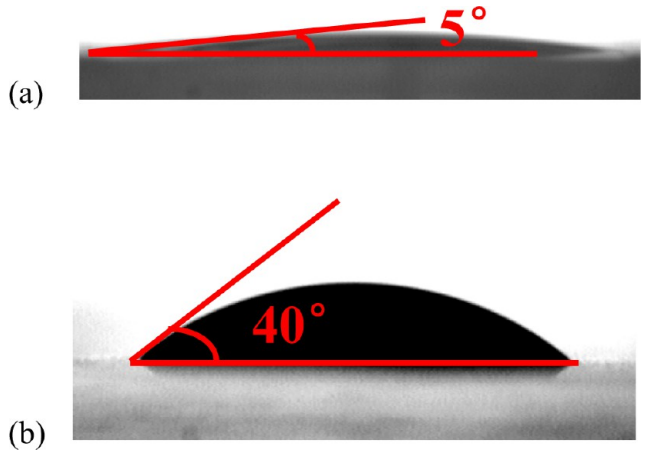


**Figure 5.** Droplets of ILs [Bmim][$PF_6$] in acetone solution on (a) M-$TiO_2$ and (b) D-$TiO_2$ films, respectively. A 5 $\mu$L drop was formed at the end of a syringe and brought into contact with the surface. Six drops were placed on each test sample, with three test samples. The results were reproducible in the range ± 1−2°.

adsorbent surface. While on D-$TiO_2$ films, with tip scanning, the rounded and nonwetting ILs [Bmim][$PF_6$] sphere tends to roll on the surface, leading to the comparable low friction coefficient. The moving liquid-like IL sphere can not interact with the $TiO_2$ surface. Therefore, it is not favorable for transmission and surface update. Only some regions of D-$TiO_2$ surface can be covered by the weakly interacted liquid-like IL, which does not act as an excellent and stable lubricant for the whole system. The remaining bare D-$TiO_2$ surface still possesses high friction coefficient.[37]

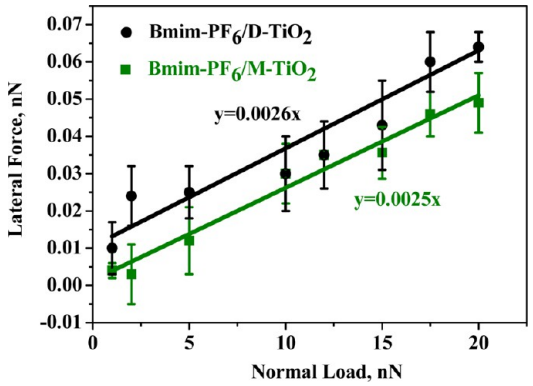


**Figure 6.** Summary of the lateral force vs normal load data recorded for ILs [Bmim][$PF_6$] on the M-$TiO_2$, D-$TiO_2$ films, and AFM tip. The slopes of the lines represent the corresponding friction coefficients.

Under $CO_2$ conditions, on M-$TiO_2$ films, it is 2 and 4 times higher $CO_2$ adsorption flux than that on D-$TiO_2$ films and pure ILs [Bmim][$PF_6$], respectively (Table 1, Figure 7a). Table 1 also indicates that the effective contact area of ILs on M-$TiO_2$ is 0.275 $m^2$, which is 2.6 times larger than that on D-$TiO_2$ (0.107 $m^2$). Apparently, the $CO_2$ transfer area has been enlarged to 2.6 times by mesoporous structure on M-$TiO_2$, further leading to the 2 times higher $CO_2$ adsorption flux. It is significant that the wetting thicknesses of ILs on M-$TiO_2$ (~5−150 nm) and D-$TiO_2$ (~400 nm) combined with the transfer area could influence the $CO_2$ adsorption rate. In Figure 7b, ILs wetted on M-$TiO_2$ enable capture rate of $CO_2$ up to 1.6 and 10 times faster than that on D-$TiO_2$ and pure ILs respectively, avoiding any significant decelerating effect through equilibrium limitations. In addition, the spreading ILs on M-$TiO_2$ reduces the time when it reaches to the maximum adsorption rate (2.8 min), faster than that on M-$TiO_2$ (6.1 min) and D-$TiO_2$ (11.2 min). Noting that $CO_2$ adsorption in equilibrium per area on M-$TiO_2$ is lower (0.16 mg $CO_2/m^2$ ILs) than that on D-$TiO_2$ (0.20 mg $CO_2/m^2$ ILs), which suggests that $CO_2$ adsorption is related not only with the wetting area, but with thickness, i, e. transfer area and diffusion distance. Therefore, the enlarged $CO_2$ transfer area and reduced diffusion distance arised from the excellent wettability of ILs, as well as the lower friction coefficient on the whole M-$TiO_2$, further accelerate the update of the surface in equilibrium to obtain a new adsorbent surface, producing highly efficient $CO_2$ capture.

**Table 1. Surface Analysis of the M-$TiO_2$ and D-$TiO_2$ Films and $CO_2$ Adsorption Parameters**

| | M-$TiO_2$ | D-$TiO_2$ | Pure ILs |
|---|---|---|---|
| surface average roughness, nm | 0.980 ± 0.05 | 0.430 ± 0.15 | |
| contact angle, deg | 40 | 5 | |
| maximum $CO_2$ adsorption rate, mg/ min | 0.0012 | 0.00074 | 0.00014 |
| time to maximum $CO_2$ adsorption rate, min | 2.8 | 6.1 | 11.2 |
| $CO_2$ adsorption flux in equilibrium, mg/ mg ILs | 0.0043 | 0.0021 | 0.0012 |
| effective contact area of ILs, $m^2$/mg ILs | 0.275 | 0.107 | |
| thickness of ILs, nm | ~5−150 | ~400 | |
| $CO_2$ adsorption in equilibrium per area, mg/ $m^2$ ILs | 0.016 | 0.020 | |

## 4. CONCLUSIONS

We have shown that when a few multilayer of ILs [Bmim][$PF_6$] are deposited on the mesoporous and dense $TiO_2$ surfaces, the whole ILs rearrange in a wetting phase on mesoporous $TiO_2$ films, but nonwetting rounded spheres on dense films. Our findings highlight the potentialities of AFM for the quantitative investigation of the interfacial properties of ILs films. On the mesoporous $TiO_2$ surface, ILs could be supported in the form of stable films. These observations could attribute to the strong adhesive force (40 nN) between ILs and mesoporous $TiO_2$ that the ILs could wet the mesoporous $TiO_2$ surface. In contrast, the adhesive force is weak (4 nN) between ILs and dense $TiO_2$ surface. Although the friction coefficient of ILs on the two $TiO_2$ surfaces are comparable as 0.0025, the rounded and nonwetting IL spheres on dense $TiO_2$ surface are apt to move along the surface, leaving the bare dense $TiO_2$ surface still highly frictional. While on the whole meosporous $TiO_2$ surface, the ILs are employed to form a stable and lowly frictional films, which is favorable for $CO_2$ adsorption in equilibrium and the surface in equilibrium to update to further obtain a new adsorbent surface. A stable ILs film wetted on mesoporous $TiO_2$ surface will increase the efficient area of ILs and shorten the $CO_2$ diffusion distance, beneficial to $CO_2$ capture rate (1.6 and 10 times faster than ILs on dense $TiO_2$ and pure ILs, respectively) and they *could* further minimize the time (just 2.8 min) to the maximum adsorption rate (shorter than that on dense $TiO_2$ and pure ILs as 6.1 and 11.2 min, respectively). This study is expected to provide a new insight for the

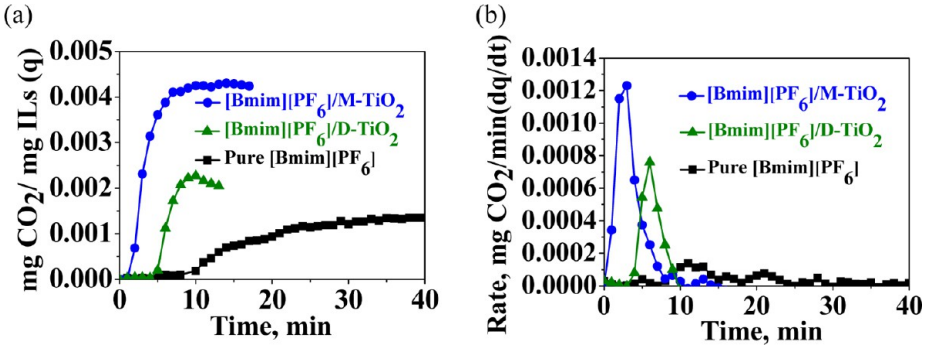


**Figure 7.** (a) Experimental $CO_2$ absorption isotherm by model ILs [Bmim][$PF_6$] [Bmim][$PF_6$] immobilized on M-$TiO_2$ and D-$TiO_2$ at 35 °C, 1 bar. (b) Rate of $CO_2$ absorption on model ILs [Bmim][$PF_6$] and [Bmim][$PF_6$] immobilized on M-$TiO_2$ and D-$TiO_2$. Note that the stoichiometry of ILs with M-$TiO_2$ and D-$TiO_2$ approaches 1:13.

development of effective methods to promote $CO_2$ adsorption and gas separation.

## AUTHOR INFORMATION


### Corresponding Author

*Tel.: +86-25-83588063 Fax: +86-25-83588063. E-mail: xhlu@njut.edu.cn.


### Notes

The authors declare no competing financial interest.

## ACKNOWLEDGMENTS

The authors are grateful for the financial support of National 973 Key Basic Research Development Planning Program (2013CB733500), Key Project of National Natural Science Foundation of China (21136004), the General Projects of the National Natural Science Foundation of China (21176112, 21206070), Colleges and Universities in Jiangsu Province plans to graduate research and innovation (CXLX12_0446). We also wish to thank Jiahua Zhu at Lamar University, Qing Shao at University of Washington, and Yihui Dong at Nanjing University of Technology for many fruitful discussions.

## REFERENCES


(1) Luo, H. M.; Dai, S.; Bonnesen, P. V.; Buchanan, A. C.; Holbrey, J. D.; Bridges, N. J.; Rogers, R. D. *Anal. Chem.* **2004**, *76*, 3078−3083.

(2) Stolte, S.; Steudte, S.; Areitioaurtena, O.; Pagano, F.; Thoming, J.; Stepnowski, P.; Igartua, A. *Chemosphere* **2012**, *89*, 1135−1141.

(3) Liu, Y.; Wang, M. J.; Li, Z. Y.; Liu, H. T.; He, P.; Li, J. H. *Langmuir* **2005**, *21*, 1618−1622.

(4) Welton, T. *Chem. Rev* **1999**, *99*, 2071−2084.

(5) Bovio, S.; Podestà, A.; Lenardi, C.; Milani, P. *J. Phys. Chem. B* **2009**, *113*, 6600-−6603.

(6) Hasib-ur-Rahman, M.; Bouteldja, H.; Fongarland, P.; Siaj, M.; Larachi, F. *Ind. Eng. Chem. Res.* **2012**, *51*, 8711−8718.

(7) Ramdin, M.; de Loos, T. W.; Vlugt, T. J. H. *Ind. Eng. Chem. Res.* **2012**, *51*, 8149−8177.

(8) Hillesheim, P. C.; Mahurin, S. M.; Fulvio, P. F.; Yeary, J. S.; Oyola, Y.; Jiang, D. E.; Dai, S. *Ind. Eng. Chem. Res.* **2012**, *51*, 11530−11537.

(9) Zhao, W.; He, G. H.; Nie, F.; Zhang, L. L.; Feng, H. C.; Liu, H. J. *J. Membr. Sci.* **2012**, *411*, 73−80.

(10) Frackowiak, E.; Lota, G.; Pernak, J. *Appl. Phys. Lett.* **2005**, *86*, 164104.

(11) Qu, J.; Truhan, J. J.; Dai, S.; Luo, H.; Blau, P. J. *Tribol. Lett* **2006**, *22*, 207−214.

(12) Nainaparampil, J. J.; Eapen, K. C.; Sanders, J. H.; Voevodin, A. A. *J. Microelectromech. Syst.* **2007**, *16*, 836−843.

(13) Nainaparampil, J. J.; Phillips, B. S.; Eapen, K. C.; Zabinski, J. S. *Nanotechnology* **2005**, *16*, 2474−2481.

(14) Zhou, F.; Liang, Y. M.; Liu, W. M. *Chem. Soc. Rev* **2009**, *38*, 2590−2599.

(15) Wasserscheid, P.; Gerhard, D.; Arlt, W. *Chem. Eng. Technol.* **2007**, *30*, 1475−1480.

(16) Kubo, W.; Kambe, S.; Nakade, S.; Kitamura, T.; Hanabusa, K.; Wada, Y.; Yanagida, S. *J. Phys. Chem. B* **2003**, *107*, 4374−4381.

(17) Pisarova, L.; Gabler, C.; Dorr, N.; Pittenauer, E.; Allmaier, G. *Tribol. Int.* **2012**, *46*, 73−83.

(18) Bhushan, B.; Palacio, M.; Kinzig, B. *J. Colloid Interface Sci.* **2008**, *317*, 275−287.

(19) Shimano, S.; Zhou, H.; Honma, I. *Chem. Mater.* **2007**, *19*, 5216−5221.

(20) Kubo, W.; Kitamura, T.; Hanabusa, K.; Wada, Y.; Yanagida, S. *Chem. Commun.* **2002**, 374−375.

(21) Stathatos, E.; Lianos, P.; Zakeeruddin, S. M.; Liska, P.; Gratzel, M. *Chem. Mater.* **2003**, *15*, 1825−1829.

(22) Susan, M. A.; Kaneko, T.; Noda, A.; Watanabe, M. *J. Am. Chem. Soc.* **2005**, *127*, 4976−4983.

(23) Neouze, M. A.; Le Bideau, J.; Leroux, F.; Vioux, A. *Chem. Commun* **2005**, 1082−1084.

(24) Szparaga, R.; Woodward, C. E.; Forsman, J. *J. Phys. Chem. C* **2012**, *116*, 15946−15951.

(25) Chen, S. F.; Jiang, S. Y. *Adv. Mater.* **2008**, *20*, 335−338.

(26) Shen, M. C.; Martinson, L.; Wagner, M. S.; Castner, D. G.; Ratner, B. D.; Horbett, T. A. *J. Biomater. Sci., Polym. Ed.* **2002**, *13*, 367−390.

(27) Leckband, D.; Sheth, S.; Halperin, A. *J. Biomater. Sci., Polym. Ed.* **1999**, *10*, 1125−1147.

(28) Zhang, X. Y.; Hua, Y. X.; Xu, C. Y.; Zhang, Q. B.; Cong, X. B.; Xu, N. *Electrochim. Acta* **2011**, *56*, 8530−8533.

(29) Flower, H. M. *Nature* **2000**, *407*, 305−306.

(30) Dalsin, J. L.; Hu, B. H.; Lee, B. P.; Messersmith, P. B. *J. Am. Chem. Soc.* **2003**, *125*, 4253−4258.

(31) Buettner, K. M.; Valentine, A. M. *Chem. Rev* **2012**, *112*, 1863−1881.

(32) Liu, X. Y.; Chu, P. K.; Ding, C. X. *Mater. Sci. Eng., R* **2004**, *47*, 49−121.

(33) Scovazzo, P.; Visser, A. E.; Davis, J. H.; Rogers, R. D.; Koval, C. A.; DuBois, D. L.; Noble, R. D. In *Ionic Liquids: Industrial Applications for Green Chemistry*, ACS Symposium Series 818; Rogers, R. D., Seddon, K. R., Eds.; American Chemical Society: Washington, DC, 2002; pp 69−87.

(34) Chen, S.; Kobayashi, K.; Kitaura, R.; Miyata, Y.; Shinohara, H. *ACS Nano* **2011**, *5*, 4902−4908.

(35) Shon, Y.-S.; Lee, S.; Colorado, R.; Perry, S. S.; Lee, T. R. *J. Am. Chem. Soc.* **2000**, *122*, 7556−7563.

(36) Lee, S.; Shon, Y.-S.; Colorado, R.; Guenard, R. L.; Lee, T. R.; Perry, S. S. *Langmuir* **2000**, *16*, 2220−2224.

(37) An, R.; Yu, Q. M.; Zhang, L. Z.; Zhu, Y. D.; Guo, X. J.; Fu, S. Q.; Li, L. C.; Wang, C. S.; Wu, X. M.; Liu, C.; Lu, X. H. *Langmuir* **2012**, *28*, 15270−15277.

(38) Zhang, L. Z.; Li, L. Y.; Chen, S. F.; Jiang, S. Y. *Langmuir* **2002**, *18*, 5448−5456.

(39) Li, W.; Bai, Y.; Liu, C.; Yang, Z. H.; Feng, X.; Lu, X. H.; van der Laak, N. K.; Chan, K. Y. *Environ. Sci. Technol.* **2009**, *43*, 5423−5428.

(40) Marchand, R.; Brohan, L.; Tournoux, M. *Mater. Res. Bull.* **1980**, *15*, 1129−1133.

(41) Li, W.; Liu, C.; Zhou, Y. X.; Bai, Y.; Feng, X.; Yang, Z. H.; Lu, L. H.; Lu, X. H.; Chan, K. Y. *J. Phys. Chem. C* **2008**, *112*, 20539−20545.

(42) Sousa, S. R.; Manuela Bras, M.; Moradas-Ferreira, P.; Barbosa, M. A. *Langmuir* **2007**, *23*, 7046−7054.

(43) Holland, N. B.; Marchant, R. E. *J. Biomed. Mater. Res.* **2000**, *51*, 307−315.

(44) Cacciafesta, P.; Hallam, K. R.; Watkinson, A. C.; Allen, G. C.; Miles, M. J.; Jandt, K. D. *Surf. Sci.* **2001**, *491*, 405−420.

(45) Zeller, A.; Musyanovych, A.; Kappl, M.; Ethirajan, A.; Dass, M.; Markova, D.; Klapper, M.; Landfester, K. *ACS Appl. Mater. Interfaces* **2010**, *2*, 2421−2428.

(46) Gelb, L. D.; Gubbins, K. E.; Radhakrishnan, R.; Sliwinska-Bartkowiak, M. *Rep. Prog. Phys.* **1999**, *62*, 1573−1659.

(47) Curry, J. E.; Zhang, F. S.; Cushman, J. H.; Schoen, M.; Diestler, D. J. *J. Chem. Phys.* **1994**, *101*, 10824−10832.